JACS
JOURNAL OF THE AMERICAN CHEMICAL SOCIETY
Article
pubs.acs.org/JACS

Side-Chain Tunability of Furan-Containing Low-Band-Gap Polymers Provides Control of Structural Order in Efficient Solar Cells

Alan T. Yiu,[†,⊥,‡] Pierre M. Beaujuge,[†,§,∥,‡] Olivia P. Lee,[†,§] Claire H. Woo,[†,⊥] Michael F. Toney,[#] and Jean M. J. Fréchet*[,†,§,⊥,∥]

[†]Materials Sciences Division, Lawrence Berkeley National Laboratory, Berkeley, California 94720, United States
Departments of [§]Chemistry and [⊥]Chemical Engineering, University of California, Berkeley, California 94720-1460, United States
[∥]King Abdullah University of Science and Technology, Thuwal, Saudi Arabia 23955-6900
[#]Stanford Synchrotron Radiation Lightsource, SLAC National Accelerator Laboratory, Menlo Park, California 94025, United States

Supporting Information

ABSTRACT: The solution-processability of conjugated polymers in organic solvents has classically been achieved by modulating the size and branching of alkyl substituents appended to the backbone. However, these substituents impact structural order and charge transport properties in thin-film devices. As a result, a trade-off must be found between material solubility and insulating alkyl content. It was recently shown that the substitution of furan for thiophene in the backbone of the polymer PDPP2FT significantly improves polymer solubility, allowing for the use of shorter branched side chains while maintaining high device efficiency. In this report, we use PDPP2FT to demonstrate that linear alkyl side chains can be used to promote thin-film nanostructural order. In particular, linear side chains are shown to shorten $\pi-\pi$ stacking distances between backbones and increase the correlation lengths of both $\pi-\pi$ stacking and lamellar spacing, leading to a substantial increase in the efficiency of bulk heterojunction solar cells.

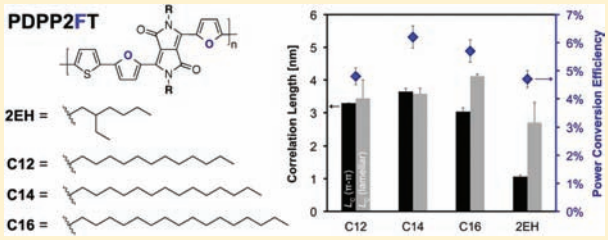

INTRODUCTION

Organic photovoltaic (OPV) technology has the potential for low-cost, high-throughput energy generation, but significant progress must be made before this potential can be realized. To date, much research has been directed toward developing low-band-gap polymer donors for use in bulk-heterojunction (BHJ) devices with fullerene-based electron acceptors.[1−9] A key goal in OPV research is to acquire a better understanding of the structure−property relationships that govern material performance. The chemical structure of a polymer donor has been shown to influence properties such as light absorption,[10−12] electronic compatibility with the fullerene acceptor,[13−17] charge transport characteristics,[18−21] thin-film morphology,[22−24] and molecular packing.[25−29] However, structural changes often have competing effects on these properties and, in turn, on device performance. In particular, while using a longer or larger solubilizing alkyl side chain generally improves solution-processability, it is also expected to increase insulating content and decrease crystallinity. Overcoming performance limitations imposed by these competing effects requires a means of optimizing one property with minimal adverse effect on other properties.

Recently, we demonstrated that furan (F) is a viable alternative to thiophene (T) in conjugated polymers for OPV applications.[29] This concept was shown using model low-band-gap polymers based on diketopyrrolopyrrole (DPP), an electron-deficient unit that has raised considerable interest for applications in transistors and solar cells.[15,30−38] From a materials design standpoint, DPP-based building blocks are particularly attractive for their scalable 3−4 step synthesis.[15,29,33] With these model polymers, we showed that incorporation of the furan co-monomer into the polymer backbone imparted markedly improved solubility. As a result, the furan-containing polymer (PDPP2FT, Figure 1) with short

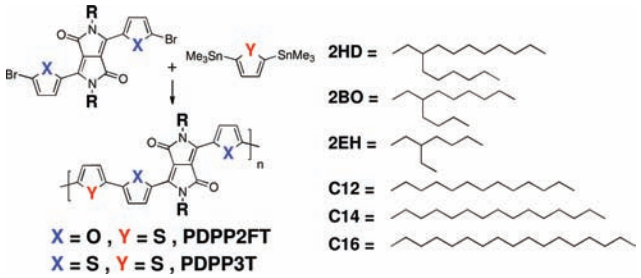

Figure 1. Synthesis of PDPP2FT derivatives with alkyl side chains of varying size and bulk.

2-ethylhexyl (2EH) side chains is processable in common organic solvents, such as tetrahydrofuran, chloroform, and chlorobenzene. In comparison, the analogous thiophene-based

Received: September 23, 2011
Published: December 22, 2011

 © 2011 American Chemical Society dx.doi.org/10.1021/ja2089662 | J. Am. Chem.Soc. 2012, 134, 2180−2185

polymer (PDPP3T, Figure 1) requires much longer 2-hexyldecyl (2HD) side chains, as previously reported by Janssen et al.[34] In BHJ devices with $PC_{71}BM$, both PDPP2FT-2EH and PDPP3T-2HD achieved comparable power conversion efficiencies (PCEs) of ca. 5%, indicating that polymer solubility could be improved while maintaining the same OPV device performance.

In parallel, it is worth noting that, as is the case with PDPP3T, the vast majority of polymer donors exhibiting high PCEs in BHJ devices have branched solubilizing side chains of various size and sterics.[16,27,39−42] While such branching centers and substituents greatly improve polymer solution-processability in organic solvents, they may not be coplanar with the backbone. We hypothesized that increasing overall polymer planarity may ultimately promote self-assembly into extended crystalline domains with longer-range backbone alignment. Increased molecular ordering in the active layer has often been shown to improve OPV performance, as a result of improved continuity of charge transport pathways.[43,44] The choice of alkyl side-chain structure has been shown to have a pronounced effect on molecular packing and, therefore, on overall device performance.[27]

In this contribution, we demonstrate that linear alkyl side chains can be used as alternatives to branched side chains in order to promote nanostructural order. The effects of side-chain structure are studied using a set of PDPP2FT derivatives, each with linear side chains of a different length. Because of the enhanced solubility of the PDPP2FT backbone, these *n*-alkyl-substituted derivatives can be solution-processed despite the absence of conventional side-chain branching. In contrast, PDPP3T derivatives with the same *n*-alkyl side chains are not soluble enough to be processed into functional devices. In agreement with our initial hypothesis, linear side chains are shown to improve structural order by reducing the $\pi-\pi$ stacking distances between backbones and increasing the correlation lengths of both $\pi-\pi$ stacking and lamellar spacing. BHJ solar cells fabricated from *n*-alkyl-substituted PDPP2FT donors exhibit PCEs reaching 6.5% (PDPP2FT-C_{14}), which is a substantial improvement over the PCEs of ca. 5% achieved with both the branched-alkyl-substituted derivative PDPP2FT-2EH and the original thiophene-based analogue PDPP3T-2HD. Thus, by leveraging the enhanced solubility imparted by the furan moiety, we show that side-chain structural design can be used to control thin-film nanostructural order and device performance. This combination of design principles paves a path to reaching PCE values exceeding those presently obtained using other thiophene-based polymer donors with branched side chains.[15,34]

RESULTS AND DISCUSSION

Synthesis and Optoelectronic Properties. To demonstrate the influence of side-chain design on structural order, PDPP2FT derivatives were synthesized with *n*-C_{12}, *n*-C_{14}, or *n*-C_{16} side chains (Figure 1). This progression of side chains was chosen in order to determine the optimal side-chain length. Synthetic details and molecular characterizations, including UV−vis absorption spectra, can be found in the Supporting Information (SI). Thin-film absorption coefficients, optical band gaps, and photoelectron spectroscopy in air (PESA)-estimated highest occupied molecular orbital (HOMO) energy levels are summarized in Table 1. The optical and electronic properties of all three derivatives are nearly identical and closely match those of the branched-alkyl-substituted analogues PDPP2FT-2EH[29] and PDDP3T-2HD.[34] The branched-alkyl-substituted derivative PDPP2FT-2BO (Figure 1) was also prepared in order to further correlate the size of the branched substituents with structural order and solar cell device performance (see SI). Further shortening the side chain to *n*-C_{10} resulted in greatly reduced solubility, and the polymerization product could not be solution-processed.

Table 1. Optical and Electrochemical Properties of PDPP2FT Polymers

derivative	extinction coefficient[a] [cm^{-1}]	optical band gap[b] [eV]	HOMO (PESA[c]) [eV]
C_{12}	1.1×10^5	1.4	−5.2
C_{14}	7.7×10^4	1.4	−5.2
C_{16}	6.5×10^4	1.4	−5.3

[a]Measured at λ_{max}. [b]Based on absorption onsets. [c]Photoelectron spectroscopy in air (PESA) measurements.

As control experiments, PDPP3T-C_{14} and -C_{16} were synthesized, but these analogues also showed limited solubility and could not be solution-processed. These findings demonstrate that the incorporation of furan in the polymer backbone allows access to polymer structures that are not otherwise soluble or processable. Previous studies comparing oligofurans to oligothiophenes have similarly reported that oligofurans and alternating furan−thiophene oligomers are more soluble than the analogous oligothiophenes.[45−47] The mechanism behind the improved solubility imparted by the furan co-monomer is not well established, but it is possible that differences in atomic radius and electronegativity between oxygen and sulfur atoms may impact solvent interactions, intermolecular interactions, and intramolecular steric interactions. It is worth noting, however, that no alkyl side chains were present in these previously reported systems.

Device Fabrication and Testing. Thin-film BHJ solar cells were fabricated using PDPP2FT-C_{12}, -C_{14}, and -C_{16} as electron donors and [6,6]-phenyl-C_{71}-butyric acid methyl ester ($PC_{71}BM$) as the electron acceptor, with a PDPP2FT:$PC_{71}BM$ blend ratio of 1:3 by weight. This blend ratio was determined for each derivative individually as part of an optimization process encompassing a wide range of device fabrication parameters (e.g., spin-coater speed, solvent, solution concentrations). The optimized device architecture was ITO/PEDOT:PSS/polymer:$PC_{71}BM$/LiF/Al. Active layers were spin-coated from chloroform solutions, with a small amount of the processing additive 1-chloronaphthalene (CN)[48] used to improve device performance.[49−51] Devices fabricated from the PDPP2FT-C_{12}, -C_{14}, and -C_{16} derivatives achieved average PCEs of 4.8%, 6.2%, and 5.7%, respectively, with PDPP2FT-C_{14} based devices reaching as high as 6.5% (Table 2). The *n*-C_{12} derivative proved relatively difficult to solution-process due to its lower solubility. The performance of the *n*-C_{14} and *n*-C_{16} derivatives, on the other hand, is substantially improved over that of the previously reported branched-alkyl-substituted analogues PDPP2FT-2EH and PDPP3T-HD, both of which achieved a PCE of ca. 5%. This PCE improvement is mostly attributed to increases in photocurrent and fill factor (FF). As shown in the device current density−voltage ($J-V$) curves and external quantum efficiency (EQE) spectra (Figure 2), PDPP2FT-C_{14}-based devices exhibit particularly high short-circuit current (J_{SC}) approaching 15 mA/cm^2 and a broad EQE spectrum approaching 50% efficiency at 500 nm. As all of the derivatives exhibit similar light absorption and electrical

dx.doi.org/10.1021/ja2089662 | J. Am. Chem.Soc. 2012, 134, 2180−2185

Table 2. PV Performance of PDPP2FT Derivatives with $PC_{71}BM$

derivative	J_{SC} [mA/cm^2]	V_{OC} [V]	FF	avg PCE ± SD [%]	max. PCE [%]
C_{12}	−12.2	0.65	0.60	4.8 ± 0.3	5.2
C_{14}	−14.8	0.65	0.64	6.2 ± 0.2	6.5
C_{16}	−12.3	0.65	0.69	5.7 ± 0.4	6.2

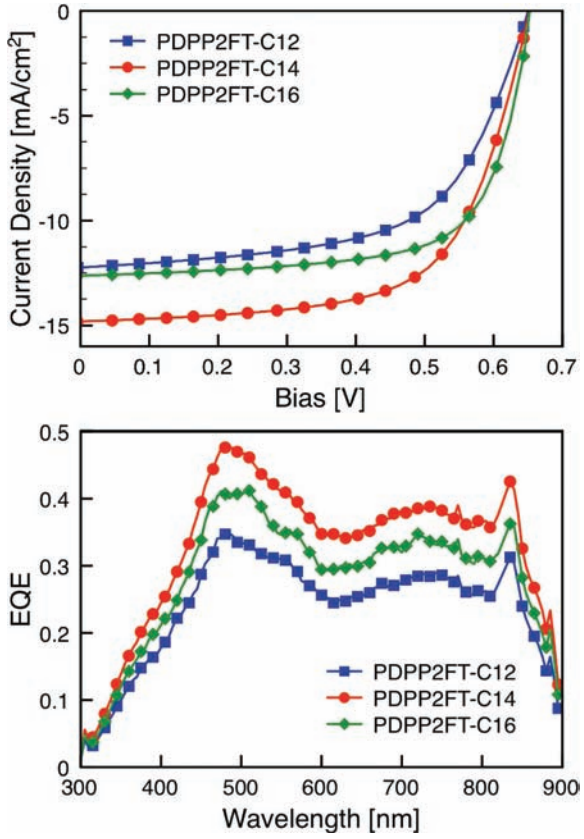

Figure 2. Average $J-V$ curves (top) and characteristic external quantum efficiency (EQE) spectra (bottom) of solar cells fabricated from PDPP2FT-C_{12}, -C_{14}, and -C_{16}.

properties, it is likely that these performance improvements are due to changes in properties such as charge carrier mobility, film morphology (donor/acceptor phase separation), and nanostructural order.

To determine the impact of side chains on charge carrier mobility, hole mobility was measured using the space charge limited current (SCLC) model. In hole-only devices (see SI), neat films of PDPP2FT-C_{12}, -C_{14}, and -C_{16} showed mobilities of 4×10^{-4}, 7×10^{-4}, and 2×10^{-3} cm^2/V-s, respectively. The high carrier mobility of these *n*-alkyl-substituted PDPP2FT derivatives is expected to contribute in part to the high photocurrents and fill factors observed in optimized BHJ devices (Figure 2). For comparison, neat films of PDPP2FT-2EH showed a hole mobility of 2×10^{-3} cm^2/V-s. Since this value is similar to the mobilities observed with PDPP2FT-C_{14} and -C_{16}, it is likely that the performance improvement seen with the *n*-alkyl-substituted derivatives arises from other thin-film parameters.

Thin-Film Morphology. As a polymer's solubilizing side chains are expected to impact its solubility and miscibility with $PC_{71}BM$, they could in turn affect the film morphology that forms during the spin-coating process. Atomic force microscopy (AFM) was used to investigate the nanoscale topography of the thin-film devices made from PDPP2FT-C_{12}, -C_{14}, and -C_{16} blended with $PC_{71}BM$ (Figure 3). Notably, all films exhibit

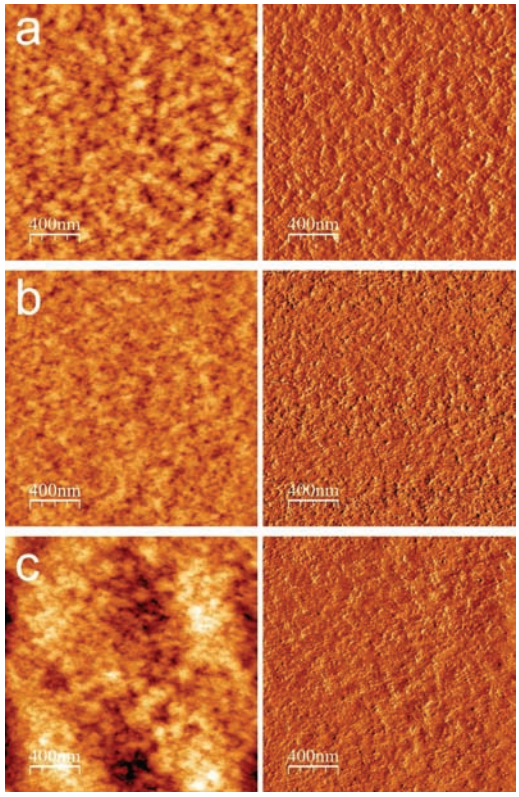

Figure 3. AFM height (left) and phase (right) images of the *n*-alkyl-substituted polymers (a) PDPP2FT-C_{12}, (b) PDPP2FT-C_{14}, and (c) PDPP2FT-C_{16}.

networks of features on the order of ca. 20 nm in size. Excitons generated in donor phases of this size scale can diffuse to a donor/acceptor interface, assuming an exciton diffusion length of ca. 10 nm.[52,53] Films of PDPP2FT-C_{12}, -C_{14}, and -C_{16} have root-mean-square (rms) roughnesses of 2.2, 1.6, and 3.3 nm, respectively. The relative smoothness of the PDPP2FT-C_{14} active layer may point to finer and more evenly distributed morphological features, which could reduce charge recombination. These results suggest that, with PDPP2FT, *n*-C_{14} side chains may provide the most adequate combination of polymer solubility and miscibility with $PC_{71}BM$ to achieve optimal film morphology. Additional studies are underway to confirm the internal morphology of the thin-film active layers.

Thin-Film Nanostructural Order. To determine the influence of side-chain substitutions on nanostructural order within the active layer, grazing-incidence X-ray scattering (GIXS) was used to examine thin-films of PDPP2FT-C_{12}, -C_{14}, -C_{16}, and -2EH, both in neat polymer films (Figure 4) and in optimized BHJ films with $PC_{71}BM$ (see SI). GIXS data can be used to determine the nature and extent of the face-to-face packing of conjugated polymer backbones ($\pi-\pi$ stacking). The

dx.doi.org/10.1021/ja2089662 | *J. Am. Chem.Soc.* 2012, 134, 2180−2185

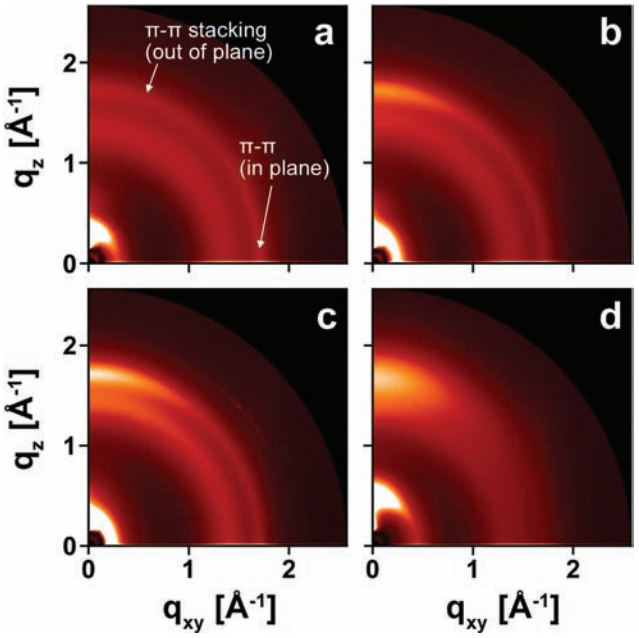

Figure 4. 2-D grazing incidence X-ray scattering (GIXS) patterns of thin films of (a) PDPP2FT-C_{12}, (b) PDPP2FT-C_{14}, (c) PDPP2FT-C_{16}, and (d) PDPP2FT-2EH.

scattering patterns of neat films of all four derivatives exhibit a $\pi-\pi$ stacking peak, visible as a ring or partial arc at $q \approx 1.7$ Å^{-1}. The stronger peak intensity near $q_{xy} \approx 0$ means that the $\pi-\pi$ stacking is preferentially oriented out-of-plane, which has been often correlated with high OPV performance.[28,54,55] As shown in Figure 4, the extent of out-of-plane orientation of each derivative increases in the order: PDPP2FT-C_{12}, -C_{14}, -C_{16}, and -2EH. This order agrees well with the SCLC hole mobilities presented earlier, as SCLC measures hole mobility in the out-of-plane direction.

In assessing the effect of these $\pi-\pi$ interactions on solar cell performance, it is important to consider π-stacking distance. A shorter distance is thought to reduce the energetic barrier for charge hopping between adjacent molecules, promoting charge transport and improving device performance.[20,56,57] Brédas and co-workers have shown in model systems that, for cofacial $\pi-\pi$ stacking, electronic couplings decay exponentially with the stacking distance and can vary by as much as a factor of 4 when the stacking distance increases from 3.4 to 4.0 Å.[20] It is expected that the solubilizing side chains of a polymer will impact this π-stacking distance. Compared to branched side chains, which create steric hindrance when polymer chains are packed tightly, linear substituents are expected to be able to organize coplanar with the backbone, allowing for closer $\pi-\pi$ stacking distances. In good agreement with this hypothesis, the π-stacking distances of PDPP2FT-C_{12}, -C_{14}, and -C_{16} are all measured to be 3.6 Å. In comparison, the π-stacking distances of PDPP2FT-2EH and -2BO are measured to be 3.7 and 3.9 Å, respectively (Table 3 and SI), suggesting that branched side chains do cause steric hindrance. Empirically, a negative correlation is observed between π-stacking distance and device performance. PDPP2FT-2BO, in particular, exhibits a much larger stacking distance (3.9 Å) and achieves the lowest solar cell performance (avg PCE of 1.3%, see SI). In parallel, it is important to note that charge transfer between two molecules also depends strongly on their in-plane offset and not just on their cofacial separation distance, as wave function overlap plays

Table 3. GIXS Peak Parameters for PDPP2FT Derivatives

	$\pi-\pi$ stacking peak		lamellar spacing peak	
derivative	d [Å]	L_C [nm]	d [Å]	L_C [nm]
C_{12}	3.6	3.3	21	3.4
C_{14}	3.6	3.6	23	3.6
C_{16}	3.6	3.0	25	4.1
2EH	3.7	1.1	13	2.7

a critical role in electronic coupling.[20] Nevertheless, as suggested by the empirical correlation drawn above, $\pi-\pi$ stacking distance provides a valuable first-order metric for evaluating the charge transport characteristics of complex polymer systems.

In addition to describing the molecular packing distances and orientation of crystallites in thin films, GIXS provides information on the extent of nanostructural order. Specifically, GIXS can be used to determine the correlation length (L_C),[25,58] which is a measure of the length scale over which one can expect a crystal lattice to be preserved. In polymer systems, order is expected to improve with the reduction of (i) the variability in chain position and rotation and (ii) the density of chain ends and lamellar folds.[56] Correlation length can be determined using the Scherrer equation,[31,32] which takes scattering peak breadth as an input. As the order of crystalline domains increases, the corresponding scattering peaks become narrower. To determine the full width at half-maximum (fwhm) peak breadths, peaks were fit to GIXS data averaged over quasi-polar angle (χ) for $\chi = 20° \pm 2°$ and $\chi = 60° \pm 2°$. The resulting average correlation lengths are shown for $\pi-\pi$ stacking and lamellar spacing peaks in Table 3 and Figure 5.

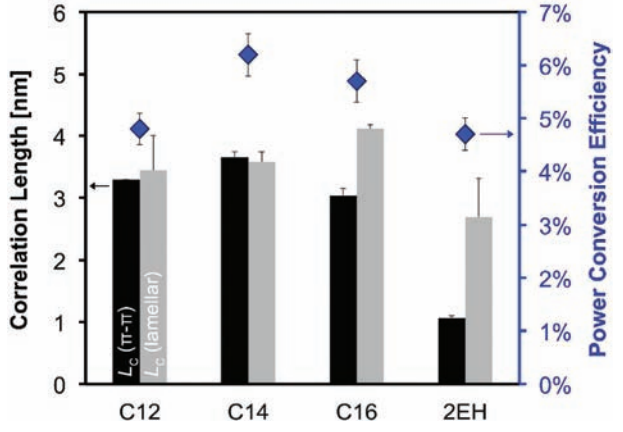

Figure 5. $\pi-\pi$ stacking (black) and lamellar spacing (gray) correlation lengths for PDPP2FT derivatives in thin-film. Power conversion efficiency in devices is shown (blue diamond) to demonstrate the relationship between $\pi-\pi$ stacking correlation length and device performance.

For ease of comparison, solar cell efficiencies (PCEs) are also reported in Figure 5. Notably, the *n*-alkyl-substituted PDPP2FT derivatives pack with significantly longer $\pi-\pi$ stacking correlation lengths (>3 nm) than does PDPP2FT-2EH (ca. 1 nm). Furthermore, device performance is substantially improved in BHJs made with PDPP2FT-C_{14}, which also shows the largest $\pi-\pi$ stacking correlation length at 3.6 nm. Recall that PDPP2FT-C_{12} had the lowest solubility of all the derivatives, which may have affected device PCE. A similar trend is observed for lamellar spacing correlation lengths, which

dx.doi.org/10.1021/ja2089662 | J. Am. Chem.Soc. 2012, 134, 2180–2185

are greater for the *n*-alkyl-substituted derivatives (ca. 3−4 nm) than for the branched-alkyl-substituted derivatives (<3 nm). Although additional studies will be required to determine the interdigitation and packing structure of the side chains, it is important to note the likely contribution of the linear chains to overall solid-state order and device performance. Increased order, particularly of $\pi-\pi$ stacking, likely minimizes the number of defects that can trap charge carriers and hinder their percolation across the active layer.[44,59] As discussed earlier, the $\pi-\pi$ stacking in these systems is preferentially oriented out-of-plane, which is also the desired direction for hole transport. As a result, the effect of $\pi-\pi$ stacking correlation length on solar cell device performance is expected to be particularly significant among factors contributing to improved performance.

CONCLUSIONS

In this report, we have demonstrated that long linear alkyl side chains can be used as alternatives to branched side chains on polymers to promote nanostructural order in thin-film solar cells. The alternating furan−thiophene PDPP2FT polymer backbone was chosen as a model system because of the significant contribution of the furan moiety to overall polymer solubility. Despite the absence of side-chain branching, solution-processability is retained in the *n*-alkyl-substituted derivatives. GIXS shows that linear side chains in these systems (i) reduce the π-stacking distances between backbones and (ii) increase $\pi-\pi$ stacking and lamellar spacing correlation lengths within polymer crystallites. Building from these design principles, we show that BHJ solar cells fabricated from *n*-alkyl-substituted PDPP2FT polymer donors and the electron-acceptor $PC_{71}BM$ exhibit PCEs reaching 6.5% (PDPP2FT-C_{14}). This high performance represents a substantial improvement over the PCE of ca. 5% achieved with the branched-alkyl-substituted derivative PDPP2FT-2EH and the original thiophene-based analogue PDPP3T-2HD.

This work demonstrates the potential of furan moieties in the design of polymer donors for efficient OPV applications. With their expanded structural design flexibility, alternating furan−thiophene low-band-gap polymers pave a path toward achieving PCE values exceeding those presently obtained with branched-alkyl-substituted thiophene-based polymer donors.

ASSOCIATED CONTENT

Supporting Information

Experimental details, synthesis of monomers and polymers, device fabrication, characterization, and complete ref 32. This material is available free of charge via the Internet at http://pubs.acs.org.

AUTHOR INFORMATION

Corresponding Author

jean.frechet@kaust.edu.sa

Author Contributions

‡These authors contributed equally.

ACKNOWLEDGMENTS

This work was supported in part by the Director, Office of Science, Office of Basic Energy Sciences, Materials Sciences and Engineering Division, of the U.S. Department of Energy under Contract No. DE-AC02-05CH11231, the Center for Advanced Molecular Photovoltaics (CAMP) under Award No. KUS-C1-015-21, supported by King Abdullah University of Science and Technology (KAUST), and the Fréchet "various gifts" fund for the support of research in new materials. Portions of this research were carried out at the Stanford Synchrotron Radiation Lightsource user facility, operated on behalf of the U.S. Department of Energy, Office of Basic Energy Sciences.

REFERENCES

(1) Thompson, B. C.; Fréchet, J. M. J. *Angew. Chem., Int. Ed.* **2008**, *47*, 58.
(2) Dennler, G.; Scharber, M. C.; Brabec, C. J. *Adv. Mater.* **2009**, *21*, 1323.
(3) Scharber, M. C.; Mühlbacher, D.; Koppe, M.; Denk, P.; Waldauf, C.; Heeger, A. J.; Brabec, C. J. *Adv. Mater.* **2006**, *18*, 789.
(4) Chen, J.; Cao, Y. *Acc. Chem. Res.* **2009**, *42*, 1709.
(5) Gunes, S.; Neugebauer, H.; Sariciftci, N. S. *Chem. Rev.* **2007**, *107*, 1324.
(6) Li, C.; Liu, M.; Pschirer, N. G.; Baumgarten, M.; Müllen, K. *Chem. Rev.* **2010**, *110*, 6817.
(7) Bundgaard, E.; Krebs, F. C. *Sol. Energ. Mater. Sol. Cells* **2007**, *91*, 954.
(8) Boudreault, P.-L. T.; Najari, A.; Leclerc, M. *Chem. Mater.* **2011**, *23*, 456.
(9) Li, Y.; Sonar, P.; Singh, S. P.; Soh, M. S.; van Meurs, M.; Tan, J. *J. Am. Chem. Soc.* **2011**, *133*, 2198.
(10) Li, Y.; Zou, Y. *Adv. Mater.* **2008**, *20*, 2952.
(11) Hou, J.; Tan, Z. A.; Yan, Y.; He, Y.; Yang, C.; Li, Y. *J. Am. Chem. Soc.* **2006**, *128*, 4911.
(12) Roncali, J. *Macomol. Rapid Commun.* **2007**, *28*, 1761.
(13) Varotto, A.; Treat, N. D.; Jo, J.; Shuttle, C. G.; Batara, N. A.; Brunetti, F. G.; Seo, J. H.; Chabinyc, M. L.; Hawker, C. J.; Heeger, A. J.; Wudl, F. *Angew. Chem., Int. Ed.* **2011**, *50*, 5166.
(14) Veldman, D.; Meskers, S. C. J.; Janssen, R. A. J. *Adv. Funct. Mater.* **2009**, *19*, 1939.
(15) Wienk, M. M.; Turbiez, M.; Gilot, J.; Janssen, R. A. J. *Adv. Mater.* **2008**, *20*, 2556.
(16) Chen, H.-Y.; Hou, J.; Zhang, S.; Liang, Y.; Yang, G.; Yang, Y.; Yu, L.; Wu, Y.; Li, G. *Nat. Photon.* **2009**, *3*, 649.
(17) Zhou, H.; Yang, L.; Price, S. C.; Knight, K. J.; You, W. *Angew. Chem., Int. Ed.* **2010**, *49*, 7992.
(18) Blom, P. W. M.; Mihailetchi, V. D.; Koster, L. J. A.; Markov, D. E. *Adv. Mater.* **2007**, *19*, 1551.
(19) Parmer, J. E.; Mayer, A. C.; Hardin, B. E.; Scully, S. R.; McGehee, M. D.; Heeney, M.; McCulloch, I. *Appl. Phys. Lett.* **2008**, *92*, 113309.
(20) Coropceanu, V.; Cornil, J.; da Silva Filho, D. A.; Olivier, Y.; Silbey, R.; Brédas, J.-L. *Chem. Rev.* **2007**, *107*, 926.
(21) Johns, J. E.; Muller, E. A.; Frechet, J. M. J.; Harris, C. B. *J. Am. Chem. Soc.* **2010**, *132*, 15720.
(22) Peet, J.; Heeger, A. J.; Bazan, G. C. *Acc. Chem. Res.* **2009**, *42*, 1700.
(23) Di Nuzzo, D.; Aguirre, A.; Shahid, M.; Gevaerts, V. S.; Meskers, S. C. J.; Janssen, R. A. J. *Adv. Mater.* **2010**, *22*, 4321.
(24) Perez, M. D.; Borek, C.; Forrest, S. R.; Thompson, M. E. *J. Am. Chem. Soc.* **2009**, *131*, 9281.
(25) Rogers, J. T.; Schmidt, K.; Toney, M. F.; Kramer, E. J.; Bazan, G. C. *Adv. Mater.* **2011**, *23*, 2284.
(26) Salleo, A.; Kline, R. J.; DeLongchamp, D. M.; Chabinyc, M. L. *Adv. Mater.* **2010**, *22*, 3812.
(27) Piliego, C.; Holcombe, T. W.; Douglas, J. D.; Woo, C. H.; Beaujuge, P. M.; Fréchet, J. M. J. *J. Am. Chem. Soc.* **2010**, *132*, 7595.
(28) Beaujuge, P. M.; Pisula, W.; Tsao, H. N.; Ellinger, S.; Müllen, K.; Reynolds, J. R. *J. Am. Chem. Soc.* **2009**, *131*, 7514.
(29) Woo, C. H.; Beaujuge, P. M.; Holcombe, T. W.; Lee, O. P.; Fréchet, J. M. J. *J. Am. Chem. Soc.* **2010**, *132*, 15547.
(30) Khlyabich, P. P.; Burkhart, B.; Ng, C. F.; Thompson, B. C. *Macromolecules* **2011**, *44*, 5079.

(31) Mei, J.; Graham, K. R.; Stalder, R.; Tiwari, S. P.; Cheun, H.; Shim, J.; Yoshio, M.; Nuckolls, C.; Kippelen, B.; Castellano, R. K.; Reynolds, J. R. *Chem. Mater.* **2011**, *23*, 2285.
(32) Bronstein, H.; et al. *J. Am. Chem. Soc.* **2011**, *133*, 3272.
(33) Walker, B.; Tamayo, A., B.; Dang, X.-D.; Zalar, P.; Seo, J. H.; Garcia, A.; Tantiwiwat, M.; Nguyen, T.-Q. *Adv. Funct. Mater.* **2009**, *19*, 3063.
(34) Bijleveld, J. C.; Zoombelt, A. P.; Mathijssen, S. G. J.; Wienk, M. M.; Turbiez, M.; de Leeuw, D. M.; Janssen, R. A. J. *J. Am. Chem. Soc.* **2009**, *131*, 16616.
(35) Loser, S.; Bruns, C. J.; Miyauchi, H.; Ortiz, R. P.; Facchetti, A.; Stupp, S. I.; Marks, T. J. *J. Am. Chem. Soc.* **2011**, *133*, 8142.
(36) Sonar, P.; Singh, S. P.; Li, Y.; Soh, M. S.; Dodabalapur, A. *Adv. Mater.* **2010**, *22*, 5409.
(37) Tamayo, A. B.; Dang, X.-D.; Walker, B.; Seo, J.; Kent, T.; Nguyen, T.-Q. *Appl. Phys. Lett.* **2009**, *94*, 103301.
(38) Bijleveld, J. C.; Karsten, B. P.; Mathijssen, S. G. J.; Wienk, M. M.; de Leeuw, D. M.; Janssen, R. A. J. *J. Mater. Chem.* **2011**, *21*, 1600.
(39) Hou, J.; Chen, H.-Y.; Zhang, S.; Li, G.; Yang, Y. *J. Am. Chem. Soc.* **2008**, *130*, 16144.
(40) Park, S. H.; Roy, A.; Beaupre, S.; Cho, S.; Coates, N.; Moon, J. S.; Moses, D.; Leclerc, M.; Lee, K.; Heeger, A. J. *Nat. Photon.* **2009**, *3*, 297.
(41) Scharber, M. C.; Koppe, M.; Gao, J.; Cordella, F.; Loi, M. A.; Denk, P.; Morana, M.; Egelhaaf, H.-J.; Forberich, K.; Dennler, G.; Gaudiana, R.; Waller, D.; Zhu, Z.; Shi, X.; Brabec, C. J. *Adv. Mater.* **2010**, *22*, 367.
(42) Hsiang-Yu, C.; Jianhui, H.; Amy, E. H.; Hoichang, Y.; Houk, K. N.; Yang, Y. *Adv. Mater.* **2010**, *22*, 371.
(43) McCulloch, I.; Heeney, M.; Bailey, C.; Genevicius, K.; MacDonald, I.; Shkunov, M.; Sparrowe, D.; Tierney, S.; Wagner, R.; Zhang, W.; Chabinyc, M. L.; Kline, R. J.; McGehee, M. D.; Toney, M. F. *Nat. Mater.* **2006**, *5*, 328.
(44) Wang, C.; Jimison, L. H.; Goris, L.; McCulloch, I.; Heeney, M.; Ziegler, A.; Salleo, A. *Adv. Mater.* **2010**, *22*, 697.
(45) Hucke, A.; Cava, M. P. *J. Org. Chem.* **1998**, *63*, 7413.
(46) Gidron, O.; Diskin-Posner, Y.; Bendikov, M. *J. Am. Chem. Soc.* **2010**, *132*, 2148.
(47) Miyata, Y.; Nishinaga, T.; Komatsu, K. *J. Org. Chem.* **2005**, *70*, 1147.
(48) Hoven, C. V.; Dang, X.-D.; Coffin, R. C.; Peet, J.; Nguyen, T.-Q.; Bazan, G. C. *Adv. Mater.* **2010**, *22*, E63.
(49) Peet, J.; Kim, J. Y.; Coates, N. E.; Ma, W. L.; Moses, D.; Heeger, A. J.; Bazan, G. C. *Nat. Mater.* **2007**, *6*, 497.
(50) Lee, J. K.; Ma, W. L.; Brabec, C. J.; Yuen, J.; Moon, J. S.; Kim, J. Y.; Lee, K.; Bazan, G. C.; Heeger, A. J. *J. Am. Chem. Soc.* **2008**, *130*, 3619.
(51) Peet, J.; Heeger, A. J.; Bazan, G. C. *Acc. Chem. Res.* **2009**, *42*, 1700.
(52) Yu, G.; Heeger, A. J. *J. Appl. Phys.* **1995**, *78*, 4510.
(53) Halls, J. J. M.; Walsh, C. A.; Greenham, N. C.; Marseglia, E. A.; Friend, R. H.; Moratti, S. C.; Holmes, A. B. *Nature* **1995**, *376*, 498.
(54) Guo, J.; Liang, Y.; Szarko, J.; Lee, B.; Son, H. J.; Rolczynski, B. S.; Yu, L.; Chen, L. X. *J. Phys. Chem. B* **2009**, *114*, 742.
(55) Beiley, Z. M.; Hoke, E. T.; Noriega, R.; Dacuña, J.; Burkhard, G. F.; Bartelt, J. A.; Salleo, A.; Toney, M. F.; McGehee, M. D. *Adv. Energ. Mater.* **2011**, in press.
(56) Street, R. A.; Northrup, J. E.; Salleo, A. *Phys. Rev. B* **2005**, *71*, 165202.
(57) Kim, Y.; Cook, S.; Tuladhar, S. M.; Choulis, S. A.; Nelson, J.; Durrant, J. R.; Bradley, D. D. C.; Giles, M.; McCulloch, I.; Ha, C.-S.; Ree, M. *Nat. Mater.* **2006**, *5*, 197.
(58) Warren, B. E. *X-Ray Diffraction*; Addison-Wesley: Reading, MA, 1969.
(59) Rivnay, J.; Noriega, R.; Northrup, J. E.; Kline, R. J.; Toney, M. F.; Salleo, A. *Phys. Rev. B* **2011**, *83*, 121306.